A massively parallel assay accurately discriminates between functionally normal and abnormal variants in a hotspot domain of *KCNH2*

Authors

Chai-Ann Ng, Rizwan Ullah, Jessica Farr, ..., Devyn W. Mitchell, Brett M. Kroncke, Jamie I. Vandenberg

Correspondence

brett.m.kroncke.1@vumc.org (B.M.K.), j.vandenberg@victorchang.edu.au (J.I.V.)

Ng et al., 2022, The American Journal of Human Genetics *109*, 1208–1216
July 7, 2022
https://doi.org/10.1016/j.ajhg.2022.05.003

CellPress

ARTICLE

A massively parallel assay accurately discriminates between functionally normal and abnormal variants in a hotspot domain of *KCNH2*

Chai-Ann Ng,[1,2,5] Rizwan Ullah,[3,5] Jessica Farr,[1,4] Adam P. Hill,[1,2] Krystian A. Kozek,[3] Loren R. Vanags,[3] Devyn W. Mitchell,[3] Brett M. Kroncke,[3,*] and Jamie I. Vandenberg[1,2,*]

Summary

Many genes, including *KCNH2*, contain "hotspot" domains associated with a high density of variants associated with disease. This has led to the suggestion that variant location can be used as evidence supporting classification of clinical variants. However, it is not known what proportion of all potential variants in hotspot domains cause loss of function. Here, we have used a massively parallel trafficking assay to characterize all single-nucleotide variants in exon 2 of *KCNH2*, a known hotspot for variants that cause long QT syndrome type 2 and an increased risk of sudden cardiac death. Forty-two percent of *KCNH2* exon 2 variants caused at least 50% reduction in protein trafficking, and 65% of these trafficking-defective variants exerted a dominant-negative effect when co-expressed with a WT *KCNH2* allele as assessed using a calibrated patch-clamp electrophysiology assay. The massively parallel trafficking assay was more accurate (AUC of 0.94) than bioinformatic prediction tools (REVEL and CardioBoost, AUC of 0.81) in discriminating between functionally normal and abnormal variants. Interestingly, over half of variants in exon 2 were found to be functionally normal, suggesting a nuanced interpretation of variants in this "hotspot" domain is necessary. Our massively parallel trafficking assay can provide this information prospectively.

Introduction

Inherited cardiac arrhythmia syndromes are the commonest cause of unexplained sudden death in 15- to 30-year-olds,[1] most often arising from rare variants in *KCNQ1* (MIM: 607542), *KCNH2* (MIM: 152427), and *SCN5A* (MIM: 600163) that cause congenital long QT syndrome[2] (MIM: 192500). Low-cost full-exome sequencing has the potential to identify individuals at risk early in life before any phenotype manifests. However, our ability to distinguish benign from pathogenic variants lags behind our ability to generate genome-sequencing data. Consequently, most missense variants identified to date are classified as variants of uncertain significance (VUSs). A VUS is not supposed to be used in clinical decision-making,[3] yet is difficult to ignore when discovered in a gene strongly associated with sudden death; as such these variants consume considerable resources in multi-disciplinary team meetings. For example, variant discovery in a "hotspot" domain of *KCNH2* is of immediate concern,[4–6] since variant location is strongly associated with increased risk of severe cardiac events.

In contrast to characterizing variants discovered in clinically identified probands and their families, *in silico* and *in vitro* experiments may prospectively identify variants that cause channel dysfunction before they are observed in individuals. Previously, characterization of variants in cardiac ion channels has relied on manual patch-clamp electrophysiology, which is prohibitively time consuming for the thousands of missense variants possible in *KCNH2*. Two recent technological developments have enabled the functional characterization of missense variants at a scale commensurate with their rate of discovery: an automated patch-clamp platform, which permits analysis of hundreds of cells simultaneously,[7–9] and massively parallel variant-effect mapping coupled to cell survival[10] or trafficking assays,[11] which measures the abundance of cell surface protein. The automated patch-clamp platform enables phenotyping of current density, gating, and permeation properties of variant channels, both homozygous and heterozygous,[9] at moderate throughput (hundreds of variants per month). Massively parallel variant effect mapping enables the analysis of tens of thousands of variants but at a reduced depth of information.[11,12] For *KCNH2*, massively parallel trafficking assays[11] have great potential, as the deleterious effects of ion channel variants in *KCNH2* are largely due to trafficking defects.[6,13]

In this work, we tested the hypotheses that (1) "hotspot" domains are enriched with functionally defective variants and (2) a massively parallel trafficking assay could distinguish functionally defective from normal variants. These assays can provide functional evidence for variant classification to reduce the burden of VUSs.

[1]Mark Cowley Lidwill Research Program in Cardiac Electrophysiology, Victor Chang Cardiac Research Institute, Darlinghurst, NSW 2010, Australia; [2]School of Clinical Medicine, UNSW Sydney, Darlinghurst, NSW, Australia; [3]Vanderbilt Center for Arrhythmia Research and Therapeutics, Division of Clinical Pharmacology, Department of Medicine, Vanderbilt University Medical Center, Nashville, TN 37232, USA; [4]School of Computer Science and Engineering, UNSW Sydney, Kensington, NSW, Australia
[5]These authors contributed equally
*Correspondence: brett.m.kroncke.1@vumc.org (B.M.K.), j.vandenberg@victorchang.edu.au (J.I.V.)
https://doi.org/10.1016/j.ajhg.2022.05.003.

Material and methods

Automated patch-clamp assay

A detailed methods paper describing the design of heterozygous *KCNH2* (GenBank: NM_000238.4) vector, generation of Flp-In T-REx HEK293 *KCNH2* variant cell lines, cell culture routine of heterozygous *KCNH2* Flp-In HEK293 for automated patch-clamp electrophysiology, operation of SyncroPatch 384PE automated patch-clamp, quality control measures, voltage protocols, and data analysis was recently published.[14] The critical components of this assay are that variants are co-expressed with the WT allele from the same plasmid that is inserted into the same place in the genome using the Flp-In recombinase technology (summarized in Figure S1). WT controls and a negative control were included together with ten *KCNH2* variants on every assay plate. Technical replicates were performed for all plates. In total, 92 assay plates (384-well) were used to collect >22,000 successful patch-clamp experiments. Current density was quantified by measuring the peak amplitude of the tail current at −50 mV, after a depolarizing step to +40 mV for 1 s. Current values were normalized to cell capacitance to obtain current density (pA/pF) and transformed to normal distribution using a square-root function before normalizing to the mean of WT from the same plate.[15]

Massively parallel trafficking assay

Mutagenesis and stable line generation

To manage *KCNH2* into workable sections, we created a tile system using the QuikChange Lightning Multi kit (Agilent), as reported earlier.[11] Specifically, the Per-Arnt-Sim (PAS) domain was included in the first of these "tiles," which we will refer to as the "PAS tile," flanked by restriction sites for ClaI and SpeI. To enable cell surface labeling of K_V11.1, a hemaglutinin (HA) tag (NSEHYPYDVP-DYAVTFE) was inserted in the region between amino acids Thr443 and Glu444, which was previously found to have no effect on the electrical or trafficking properties of the channel.[16] We completed a comprehensive site saturation mutagenesis on the PAS tile with mutagenic primer pairs comprising a 5′ NNN segment on the forward primer, where N is a mix of A/C/G/T, and then added these mutagenized segments into the full-length construct as previously described.[11] Results were analyzed using in-house Python and R scripts. Transfecting and creating a stable cell line and preparing cells for flow sorting followed the same protocol as previously described (see also the supplemental methods).[11]

NovaSeq sequencing of the generated libraries

DNA was isolated from each pool of cells sorted for extracellular staining using 100 μL QuickExtract (Lucigen) per 1 million cells, following the manufacturer's instructions. Polymerase chain reaction (PCR) was used to amplify the barcode, and the resulting products were purified with AMPure XP beads (Beckman Coulter), following the manufacturer's instructions. The libraries were sequenced on a NovaSeq 6000 instrument with 150-base paired-end sequencing. (For more details, see the supplemental methods.)

Variant counts from each pool of sorted cells were aggregated to calculate a trafficking score using the following equation:

$$\textit{Trafficking score}_i = \frac{1*(\textit{Pool}_{1,i}) + 2*(\textit{Pool}_{2,i}) + 3*(\textit{Pool}_{3,i}) + 4*(\textit{Pool}_{4,i})}{\textit{Total number of barcodes observed}_i} \quad \text{(Equation 1)}$$

Where $\text{Pool}_{n,i}$ is the fraction of the i^{th} barcode in the n^{th} pool of sorted cells; n ranges from 1 (no K_V11.1 present, i.e., no Alexa Fluor 647 [AF647] signal) to 4 (high abundance of K_V11.1, i.e., high AF647 signal). The scores were then aggregated by variant and normalized with a linear transformation so that trafficking score ranged from 0 (barcodes only observed in the AF647-negative pool) to 100 for WT. The scores were then averaged across the two replicate experiments (separate transfections of the mutant library pool). A total of 1,449 observed out of 1,463 total possible missense variants, 77 synonymous, and 77 nonsense variants were assayed for trafficking phenotype (Figure 1).

Replicates

Two mutagenized plasmids with unique barcode-variant associations were generated and transfected into three separate HEK293 cell lines for a total of six biological replicates. Within each plasmid, there were approximately 2–9 (interquartile range) technical replicates, owing to the redundancy of barcodes and codon substitutions associated with the same missense variant.

Modeling peak tail current

Models included Rare Exome Variant Ensemble Learner (REVEL),[17] CardioBoost,[18] and/or high-throughput trafficking data where mentioned. Logistic regression models to evaluate AUCs (areas under the receiver operating characteristic [ROC] curve) were built using the glm function in the rms package in R. Confidence intervals were calculated using a 1,000× bootstrap with resampling.

Ethics declaration

No patient data were used in this study, and therefore institutional review board approval was not required.

Results

Massively parallel trafficking assay

Pathogenic missense variants throughout the proteome are most often caused by destabilization-induced misfolding;[19–22] for *KCNH2*, this results in loss of trafficking to the plasma membrane.[5,6,23] Here, we investigated all codon substitutions in exon 2 of *KCNH2* (Figure S2 denotes its location within the protein), one of the hotspots for pathogenic variants,[4–6] with a massively parallel trafficking assay (Figure 1). We use "trafficking" here to indicate surface expression; however, low overall channel expression in heterologous cells may underly a small proportion of trafficking-defective variants. Trafficking scores were calculated by counting variants in pools of sorted cells as previously described[11] and detailed in the material and methods. The trafficking scores ranged between 0% and 160% of WT for the 1,449/1,463 homozygous missense variants identified, 0%–165% of WT for the 77 synonymous variants (median of 100% of WT by definition), and 0% of WT for the 77 nonsense variants (median of 0% of WT; Figure 1). Though the trafficking distribution of synonymous variants is largely like WT, there were two outliers (p.Asp46= and p.His70=) that were tested separately and found to traffic like WT, indicating a limitation to the method (Figure S3). The observed distribution of the trafficking scores for missense variants was bimodal with peaks around 0 and 100 (Figure 1B). Figure 1C shows a summary heatmap of the observable

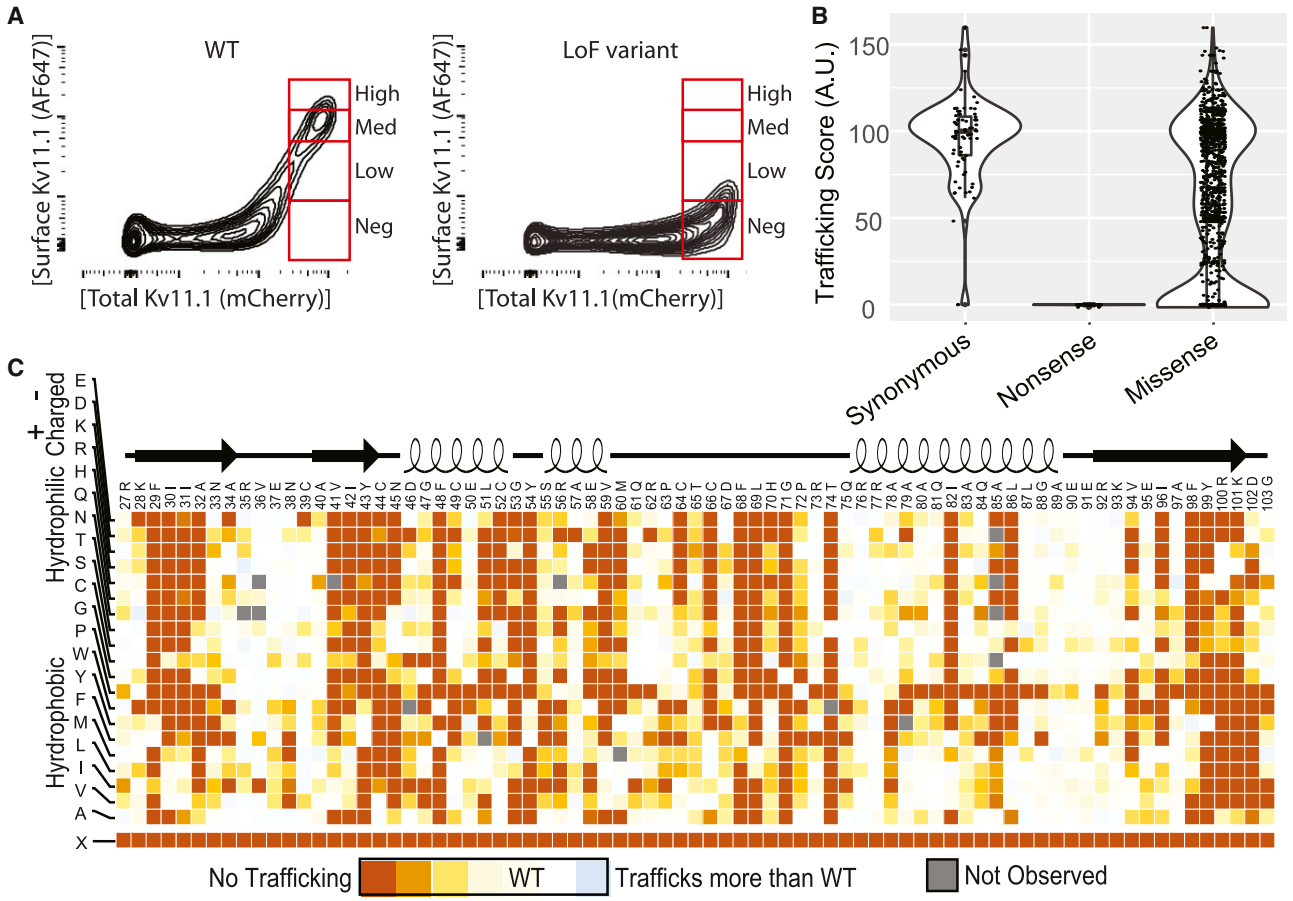

Figure 1. Deep mutational scan of exon 2 of *KCNH2* identifying trafficking-deficient variants
(A) Fluorescence-activated cell sorting plots of wild-type (WT) *KCNH2* and a loss-of-function (LoF) variant.[11] Cell surface concentration of Alexa Fluor 647 (AF647)-labeled K_V11.1 (encoded by *KCNH2*), a correlate of trafficking, is shown in the y axis; bins indicate populations of cells with high, medium (med), low, and negative (neg) AF647 surface staining. Expression of *KCNH2* is inferred by mCherry fluorescence (expressed on the same transcript) plotted on the x axis (see material and methods for details).
(B) Violin plots showing the trafficking scores for all synonymous, nonsense, and missense variants in the exon 2 region.
(C) Trafficking levels, normalized to the median synonymous value and color coded on a converging scale, for the 1,603 variants assayed. Regions corresponding to structural elements are denoted by solid arrows (β sheets) and coils (α helices) at the top of the panel.

trafficking scores with deleterious variants concentrated around the structural regions of the protein.

Large-scale automated patch-clamp assay

For our automated patch-clamp assays of heterozygous *KCNH2* variants, we characterized the subset of 458 non-redundant missense single-nucleotide variants (SNVs; the most common type of clinically observed variant) in exon 2. Typical examples of tail currents from WT and a selection of 10 variants stably expressed in Flp-In HEK293 cell lines (and a negative control) recorded on the same 384-well plate are shown in Figure 2A. The current densities recorded at −50 mV are presented as violin plots in Figure 2B. The normalized current density measured at −50 mV is similar to −120 mV (Figure S4). The mean values for all 458 variants are categorized into three groups (severe functional defect, <32%; partial functional defect, 32%–61%; and functionally normal, >61% of WT) based on previously established thresholds[15] calibrated according to recommendations from the Clinical Genome (ClinGen) Sequence Variant Interpretation (SVI) Working Group,[24] are summarized in Figure 2C. Figure 2D shows the current densities of exon 2 variants found in gnomAD, and the majority (22 of 25) are functionally normal. There were 118 exon 2 variants found in the ClinVar database (https://www.ncbi.nlm.nih.gov/clinvar/): 2 have been classified as likely benign (p.Ala34Val [c.101C>T] and p.Lys93Arg [c.278A>G]), 42 have been classified as VUSs without conflicting, and a further 74 do not have classification provided (Table S1). The current densities for these ClinVar VUSs spread across the functionally normal and abnormal ranges, whereas the majority of the ClinVar "not provided" variants show a distribution similar to the likely pathogenic variants reclassified including functional data in a recent study.[15]

There were 125 of 458 variants with <32% of WT current density, which precluded analysis of their gating kinetics. Of the 65 of 458 variants that show partial loss of current density (between 32% and 61% of WT), 10 have abnormal deactivation (Figure S5). Of the 268 of 458 variants that

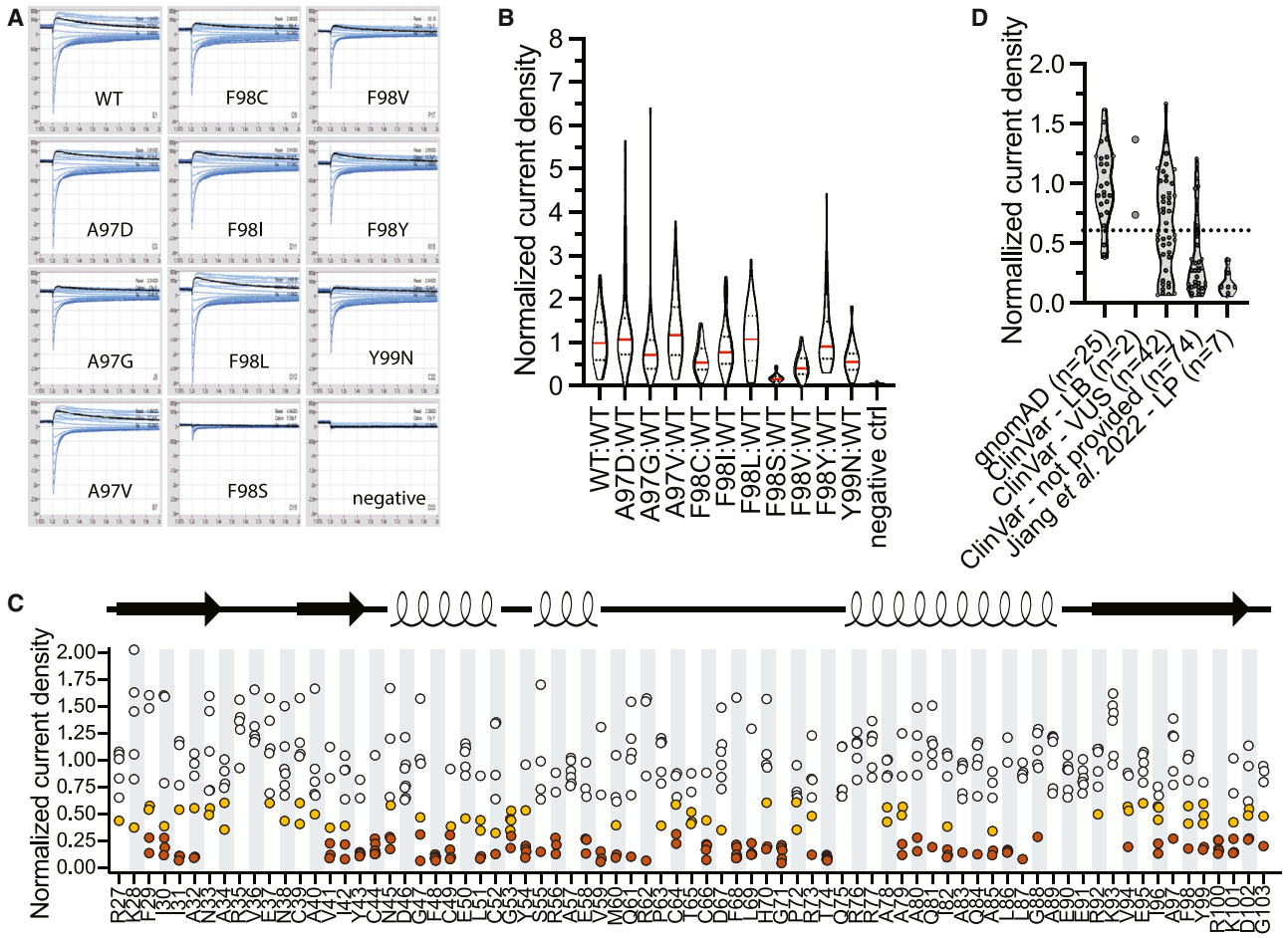

Figure 2. Functional phenotyping of all missense SNVs in exon 2 of *KCNH2* using automated patch-clamp (APC)

(A) A family of peak tail current traces correspond to WT:WT (1), p.Ala97Asp:WT (2), p.Ala97Gly:WT (3), p.Ala97Val:WT (4), p.Phe98Cys:WT (5), p.Phe98Ile:WT (6), p.Phe98Leu:WT (7), p.Phe98Ser:WT (8), p.Phe98Val:WT (9), p.Phe98Tyr:WT (10), p.Tyr99Asn:WT (11), and a negative control (12). The highlighted black peak tail currents were acquired after depolarization at +40 mV for 1 s before stepping to −50 mV.

(B) The violin plots for the normalized −50 mV peak tail current density that correspond to those variants shown in (A).

(C) The normalized peak tail current density of all the missense SNVs. The number of cells used to derive these mean values ranged from n = 13 to n = 56 for each variant, with an average of n = 39. The different levels of peak tail current density are categorized as functionally normal (>61% of WT; white; 268 variants), functionally abnormal with partial loss of function (32%–61% of WT; orange; 64 variants), and functionally abnormal with severe loss of function (<32% of WT; brown; 126 variants).

(D) Normalized current density for gnomAD variants, existing likely benign and VUS/not provided in ClinVar, and the likely pathogenic variants classified recently in Jiang et al.[15] All data for these 458 variants are provided in Table S1.

have current density within the normal range (>61% of WT), only 23 have abnormal gating (Figure S5 and Table S1).

For the subset of 458 non-redundant, missense SNVs, the trafficking and peak tail current density measurements were similar (Figures 3A, 3B, and 4C), with both showing bimodal distributions (Figure 3Ci). When these SNVs were expressed homozygously, 42% show a reduction in protein trafficking of at least 50% (moderate to severe). Sixty-five percent of these moderate to severe trafficking-defective variants also resulted in current density values that were less than 32% of WT measured by the heterozygous patch-clamp assay. This indicates that more than half of the trafficking-defective variants also have a dominant-negative effect on the co-expressed WT allele (Figures 3A and 3B). The deleterious variants were distributed in clusters on the K_V11.1 structure (Figure 3Cii) that are either buried or located on the surface that binds to the cyclic nucleotide binding homology (cNBH) domain;[25] residues more tolerant to substitution mapped to the periphery of these clusters (Figure 3Cii).

A comparison between bioinformatic predictions and functional data

The ACMG/AMP guidelines[3] for variant classification suggest that predictions from *in silico* tools can provide supporting evidence (BP4/PP3) for variant pathogenicity, in contrast to strong evidence (BS3/PS3) for functional data. Consistent with this distinction, we found a moderate correlation between measured peak tail current

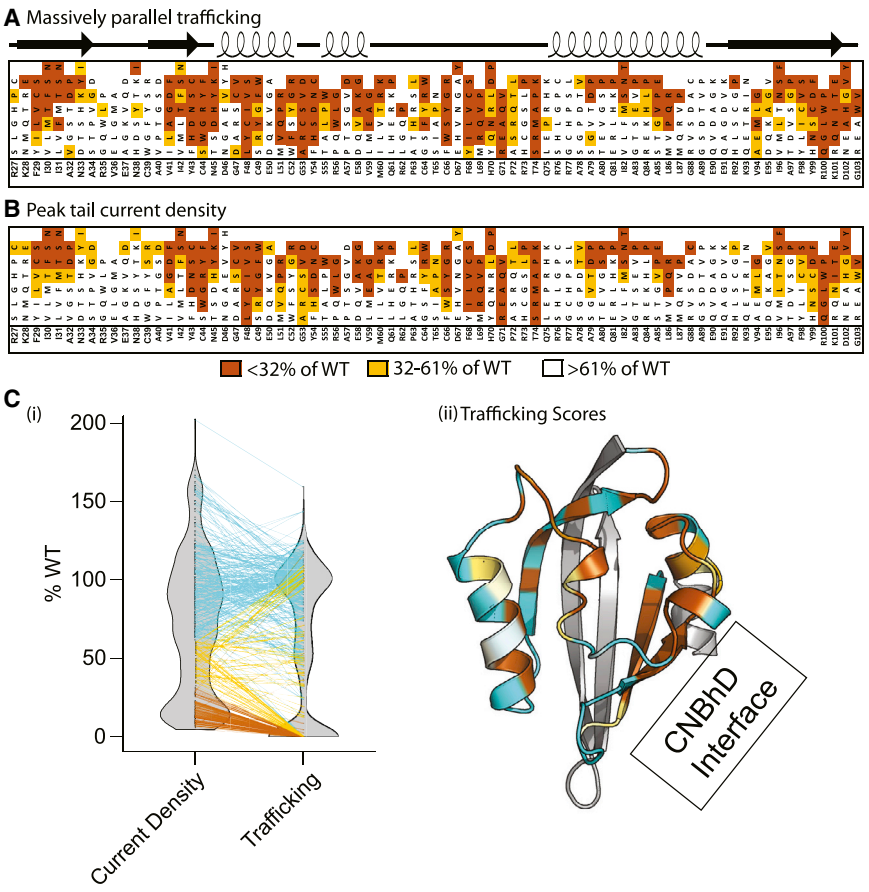

Figure 3. Concordance between massively parallel trafficking assay and peak tail current density; preponderance of functionally "benign" variants in exon 2 "hotspot" of *KCNH2*

(A and B) Impaired trafficking of homozygous missense SNVs (A) and peak tail current density for heterozygous missense SNVs (B) are color coded as having <32% of WT (brown), 32%–61% of WT (orange), and >61% of WT (white).

(Ci) Violin plots showing the peak tail current density and massively parallel trafficking scores for all SNVs in exon 2. Lines between the violin plot are the peak tail current density and massively parallel trafficking scores for each SNV, color coded based on the thresholds established using the automated patch-clamp assay.

(Cii) Massively parallel trafficking assay results mapped onto the structure of the PAS domain (PDB: 5VA1). The orange/brown color scale is the same as in (A) and (B). Regions tolerant of substitution are shown in cyan. The box to the bottom right indicates the PAS-cNHB domain interaction surface.

density and levels predicted by the commonly used *in silico* variant classifiers, REVEL[17] and CardioBoost,[18] both with a Spearman ρ ~0.5 (Figures 4A and 4B). Trafficking results were much more correlated with measured peak tail current density (Figure 4C), Spearman $\rho = 0.77$, 95% confidence interval: 0.73–0.81. A model predicting peak tail current density using REVEL and CardioBoost alone had a coefficient of determination, adjusted for the number of regression features, of $R^2 = 0.29$, 0.23–0.37 ($p < 0.001$), also suggesting modest overlap of information. In contrast, a model using high-throughput trafficking data alone produced an $R^2 = 0.66$, 0.61–0.72 ($p < 0.001$); adding REVEL and CardioBoost to the trafficking data did not improve models compared to models based on the trafficking feature alone ($R^2 = 0.66$ [0.62–0.71]). AUCs using REVEL and CardioBoost to classify variants had similar predictive accuracy (AUC of 0.81, Figures 4D and 4E); this performance persisted across multiple cut-offs of pathogenicity (Figure 4E). The trafficking data substantially outperformed all other features (Figure 4), correctly classifying loss-of-function variants with an AUC of 0.94 (Figure 4E). Adding REVEL and CardioBoost to the trafficking data did not improve predictive ability (AUC = 0.95, logistic regression model as described in the material and methods) (Figure 4E). These results indicate that the trafficking data contain new information absent in REVEL and CardioBoost.

Discussion

Here, we compared and validated a massively parallel trafficking assay against a high-information-content, automated patch-clamp assay for assessing variants in *KCNH2*. The schematic for the massively parallel trafficking assay and automated patch-clamp assay are described in Figure S1.

Out of all the SNVs located in exon 2 that we assessed, 42% produce less than 50% protein trafficking, and 65% of these trafficking-deficient variants also exerted a dominant-negative effect by reducing the current density when co-expressed with a WT subunit. Defective gating was only a minor contributor to the overall deleterious effect for exon 2 variants. These deleterious variants were typically found in clusters when mapped onto the PAS domain; variants that largely tolerate substitution were found on the periphery of these clusters. Finally, peak tail current density phenotype was very well predicted by the trafficking data, whereas *in silico* variant tools[17,18] provided little additional information for these predictions.

Like earlier studies,[9,11] we observed significant variability in the extent of deleterious effects for missense variants (Figures 1C and 2C). A structure-based analysis of the functional impact of variants shows that loss-of-function variants were distributed throughout the PAS domain, though they were denser in certain pockets (Figure 3Cii). As expected, buried regions were generally intolerant of substitutions,[21] whereas solvent-exposed regions were generally tolerant (Figure 3Cii). The deleterious *KCNH2* variants identified in our study are generally consistent with those quantified

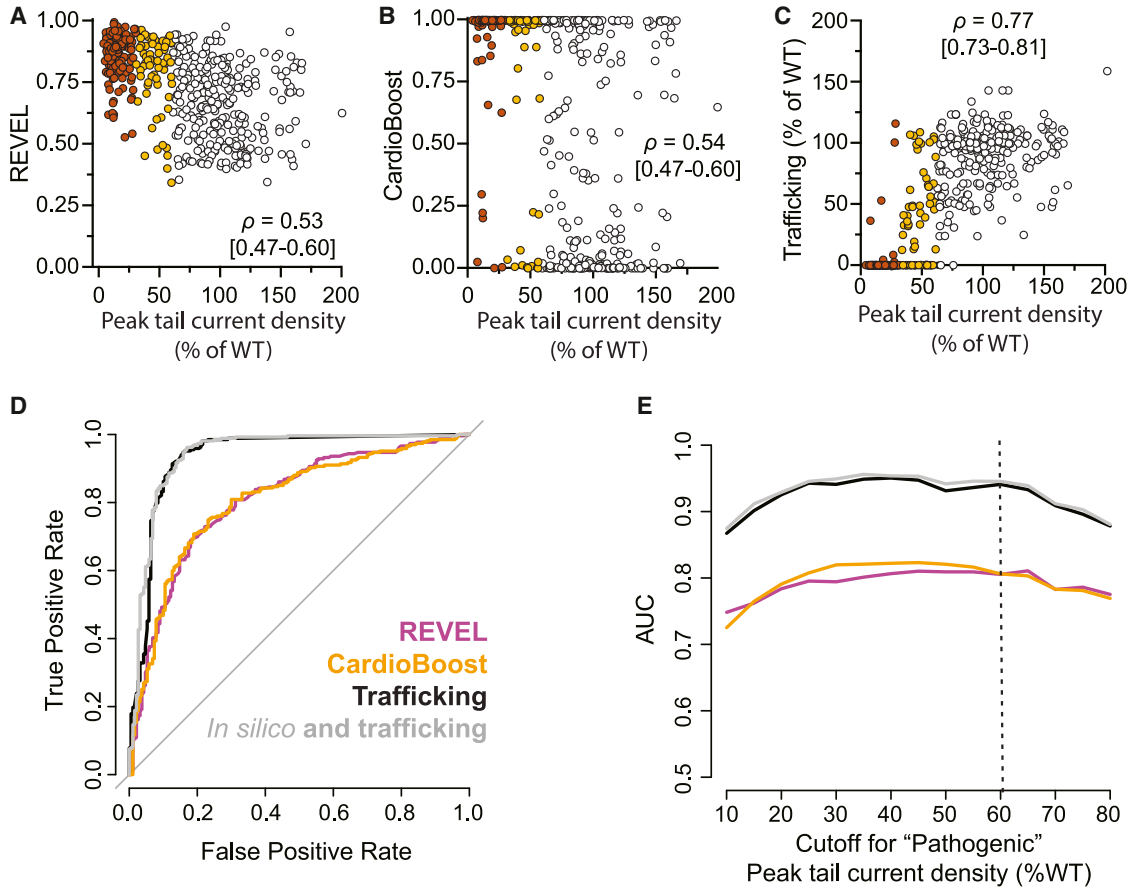

Figure 4. Massively parallel trafficking data accurately recapitulate peak tail current density

(A–C) Correlations between heterozygous peak tail current density and REVEL score (A), CardioBoost (B), and massively parallel trafficking assay (C). Variants are color coded based on the peak tail current density: 0%–32% of WT (brown), 32%–61% of WT (orange), and >61% of WT (white). Spearman rank-order correlations, ρ, are shown in the inset, with bootstrap-resampled 95% confidence intervals shown in brackets (2.5%–97.5%) (see material and methods).

(D) ROC curves for predicting less than 61% of WT peak tail current density for exon 2 missense SNVs.

(E) Areas under the ROC curve (AUCs) calculated at multiple cut-offs of "pathogenicity," loss of peak tail current density. The dashed vertical line indicates the 61% of WT cut-off value. Light gray indicates a logistic regression to peak current data, which includes trafficking data and both REVEL and CardioBoost (see material and methods). These results indicate that the trafficking data recapitulate and expand upon the information relevant to predicting peak tail current obtained from *in silico* predictors.

using a western blot assay[26] (Figure S6A; Spearman rank-order correlations of 0.93) or a PAS domain protein-solubility assay[27] (Figure S6B; Spearman rank-order correlations of 0.80). However, significant advantages of our parallel trafficking assay are that it is capable of greater throughput and it can be applied to the full-length channel. The PAS domain, which is partly encoded by exon 2 of *KCNH2*, has been previously shown to cause abnormal deactivation gating.[25,28] Even though our massively parallel trafficking assay does not measure channel gating, only 10% of those heterozygous variants that have sufficient current density (>32% of WT) to permit a reliable gating analysis have shown an accelerated channel deactivation measured by patch-clamp assay (Figure S5). This is consistent with impaired trafficking to the plasma membrane being the major defect for most of the deleterious *KCNH2* variants.[6]

The high sensitivity but low specificity of *in silico* tools, as shown in Figure 4 and previous studies,[29] is one reason the ACMG/AMP variant interpretation guidelines suggest *in silico* data be interpreted as supporting evidence (BP4/PP3) of variant pathogenicity compared to strong evidence (BS3/PS3) for functional data.[3] The greater accuracy of the trafficking data in predicting loss of function, compared to the REVEL and CardioBoost *in silico* tools,[17,18] indicates that the trafficking assay provides information that is not present in these *in silico* predictors. The *in silico* criterion (PP3) often affects the final classification of pathogenic/likely pathogenic variants,[30] and it has been suggested that properly calibrated *in silico* criteria (i.e., REVEL score ≥0.8) may be used at a moderate evidence level.[30] For *KCNH2*, we have shown that the correlation between REVEL scores and functional data is only moderate ($\rho \sim 0.5$). Also, there are 62 variants that are scored ≥0.8 for REVEL (i.e., deleterious) (Figure 4A) but are functionally normal, i.e., they had >61% of WT current density, which is the threshold determined using a set of classified benign and pathogenic variant controls for differentiating normal from abnormal function[15]. We therefore suggest a cautious

approach should be taken when applying *in silico* tools to *KCNH2* variants.

The mutational hotspot criterion (PM1) has also been applied to variants located within exon 2 of *KCNH2*;[31] however, we have shown that a large proportion of variants within exon 2 of *KCNH2* are functionally normal (Figure 3). If PM1 criteria were applied to functionally normal variants, they would not be classified as likely benign due to the conflicting criteria: functionally normal (BS3) versus mutational hotspot (PM1). We therefore urge caution in assuming that all variants in a "hotspot" domain are likely pathogenic and suggest that a more nuanced approach needs to be taken. This is likely to be of particular importance for assessing patients with incidental findings of a variant in a known "hotspot." However, it is also important to point out that the HEK293 cell line may not have the complex regulatory processes, as a recent study has shown that PAS domain variants may have different phenotypes when co-expressed with the *KCNH2* isoform (hERG1b) in cardiomyocytes derived from induced pluripotent stem cells (iPSCs).[32] Furthermore, the trafficking assay, though an exceptional improvement over currently used *in silico* predictors, still produces false positives at a non-zero rate (Figures 1B and S3).

Identifying genetic variants that cause clinically relevant phenotypic changes is a barrier to realizing the promise of genome-guided medicine. Prospectively classifying variants has the potential to bring us closer by drastically reducing the delay between acquiring a genome-sequencing result and establishing a diagnosis. These new data will also permit a more nuanced interpretation of the variant-induced LQTS diagnosis probability.[4] We suggest the assays described here will enable the prospective collection of meaningful functional data for all missense variants in *KCNH2*.

Data and code availability

The raw data that support the findings of this study are available at https://doi.org/10.5061/dryad.zpc866t9x for patch-clamp experiments and https://doi.org/10.5061/dryad.dbrv15f3f for parallel trafficking experiments. The corresponding analysis scripts for patch-clamp experiments are available at https://git.victorchang.edu.au/projects/SADA/repos/syncropatch_automated_analysis/browse, and in-house Python and R scripts to associate barcodes and variants across the tile for the parallel trafficking are available at https://github.com/kroncke-lab/KCNH2_DMS. The trafficking and patch-clamp results for the 458 SNVs are available in Table S1.

Supplemental information

Supplemental information can be found online at https://doi.org/10.1016/j.ajhg.2022.05.003.

Acknowledgments

This work was funded by an NSW Cardiovascular Disease Senior Scientist grant (J.I.V.), an National Health and Medical Research Council Principal Research Fellowship (J.I.V.), National Institutes of Health grant R00HL135442 (B.M.K.), Leducq Foundation for Cardiovascular Research grant 18CVD05 "Toward Precision Medicine with Human iPSCs for Cardiac Channelopathies" (B.M.K.), and American Heart Association Career Development Award 848898 (B.M.K.). We also acknowledge support from the Victor Chang Cardiac Research Institute Innovation Centre, funded by the NSW Government.

Author contributions

Conceptualization: B.M.K., J.I.V.; Data curation: C.-A.N., R.U., L.R.V., D.W.M.; Formal Analysis: C.-A.N., R.U., K.A.K., A.P.H., B.M.K., J.I.V.; Funding acquisition: B.M.K., J.I.V.; Methodology: J.F., A.P.H., R.U., D.W.M., L.R.V., B.M.K., J.I.V.; Writing – original draft: C.-A.N., R.U., A.P.H., B.M.K., J.I.V.; Writing – review & editing: C.-A.N., R.U., B.M.K., J.I.V.

Declaration of interests

The authors declare no competing interests.

Received: January 10, 2022
Accepted: May 3, 2022
Published: June 9, 2022

References

1. Bagnall, R.D., Weintraub, R.G., Ingles, J., Duflou, J., Yeates, L., Lam, L., Davis, A.M., Thompson, T., Connell, V., Wallace, J., et al. (2016). A prospective study of sudden cardiac death among children and young adults. N. Engl. J. Med. *374*, 2441–2452. https://doi.org/10.1056/NEJMoa1510687.
2. Priori, S.G., Wilde, A.A., Horie, M., Cho, Y., Behr, E.R., Berul, C., Blom, N., Brugada, J., Chiang, C.E., Huikuri, H., et al. (2013). HRS/EHRA/APHRS expert consensus statement on the diagnosis and management of patients with inherited primary arrhythmia syndromes. Heart Rhythm *10*, 1932–1963. https://doi.org/10.1016/j.hrthm.2013.05.014.
3. Richards, S., Aziz, N., Bale, S., Bick, D., Das, S., Gastier-Foster, J., Grody, W.W., Hegde, M., Lyon, E., Spector, E., et al. (2015). Standards and guidelines for the interpretation of sequence variants: a joint consensus recommendation of the American college of medical genetics and genomics and the association for molecular pathology. Genet. Med. *17*, 405–424. https://doi.org/10.1038/gim.2015.30.
4. Kozek, K., Wada, Y., Sala, L., Denjoy, I., Egly, C., O'Neill, M.J., Aiba, T., Shimizu, W., Makita, N., Ishikawa, T., et al. (2021). Estimating the posttest probability of long QT syndrome diagnosis for rare *KCNH2* variants. Circ. Genom Precis Med. *14*, e003289. https://doi.org/10.1161/circgen.120.003289.
5. Smith, J.L., Anderson, C.L., Burgess, D.E., Elayi, C.S., January, C.T., and Delisle, B.P. (2016). Molecular pathogenesis of long QT syndrome type 2. J. Arrhythm *32*, 373–380. https://doi.org/10.1016/j.joa.2015.11.009.
6. Anderson, C.L., Kuzmicki, C.E., Childs, R.R., Hintz, C.J., Delisle, B.P., and January, C.T. (2014). Large-scale mutational analysis of Kv11.1 reveals molecular insights into type 2 long QT syndrome. Nat. Commun. *5*, 5535. https://doi.org/10.1038/ncomms6535.

7. Vanoye, C.G., Desai, R.R., Fabre, K.L., Gallagher, S.L., Potet, F., DeKeyser, J.M., Macaya, D., Meiler, J., Sanders, C.R., and George, A.L., Jr. (2018). High-throughput functional evaluation of *KCNQ1* decrypts variants of unknown significance. Circ. Genom Precis Med. *11*, e002345. https://doi.org/10.1161/circgen.118.002345.
8. Glazer, A.M., Wada, Y., Li, B., Muhammad, A., Kalash, O.R., O'Neill, M.J., Shields, T., Hall, L., Short, L., Blair, M.A., et al. (2020). High-throughput reclassification of *SCN5A* variants. Am. J. Hum. Genet. *107*, 111–123. https://doi.org/10.1016/j.ajhg.2020.05.015.
9. Ng, C.A., Perry, M.D., Liang, W., Smith, N.J., Foo, B., Shrier, A., Lukacs, G.L., Hill, A.P., and Vandenberg, J.I. (2020). High-throughput phenotyping of heteromeric human ether-a-go-go-related gene potassium channel variants can discriminate pathogenic from rare benign variants. Heart Rhythm *17*, 492–500. https://doi.org/10.1016/j.hrthm.2019.09.020.
10. Findlay, G.M., Daza, R.M., Martin, B., Zhang, M.D., Leith, A.P., Gasperini, M., Janizek, J.D., Huang, X., Starita, L.M., and Shendure, J. (2018). Accurate classification of *BRCA1* variants with saturation genome editing. Nature *562*, 217–222. https://doi.org/10.1038/s41586-018-0461-z.
11. Kozek, K.A., Glazer, A.M., Ng, C.A., Blackwell, D., Egly, C.L., Vanags, L.R., Blair, M., Mitchell, D., Matreyek, K.A., Fowler, D.M., et al. (2020). High-throughput discovery of trafficking-deficient variants in the cardiac potassium channel KV11.1. Heart Rhythm *17*, 2180–2189. https://doi.org/10.1016/j.hrthm.2020.05.041.
12. Glazer, A.M., Kroncke, B.M., Matreyek, K.A., Yang, T., Wada, Y., Shields, T., Salem, J.E., Fowler, D.M., and Roden, D.M. (2020). Deep mutational scan of an *SCN5A* voltage sensor. Circ. Genom Precis Med. *13*, e002786. https://doi.org/10.1161/circgen.119.002786.
13. Delisle, B.P., Anson, B.D., Rajamani, S., and January, C.T. (2004). Biology of cardiac arrhythmias: ion channel protein trafficking. Circ. Res. *94*, 1418–1428. https://doi.org/10.1161/01.res.0000128561.28701.ea.
14. Ng, C.A., Farr, J., Young, P., Windley, M.J., Perry, M.D., Hill, A.P., and Vandenberg, J.I. (2021). Heterozygous *KCNH2* variant phenotyping using Flp-In HEK293 and high-throughput automated patch clamp electrophysiology. Biol. Methods Protoc. *6*, bpab003. https://doi.org/10.1093/biomethods/bpab003.
15. Jiang, C., Richardson, E., Farr, J., Hill, A.P., Ullah, R., Kroncke, B.M., Harrison, S.M., Thomson, K.L., Ingles, J., Vandenberg, J.I., et al. (2022). A calibrated functional patch-clamp assay to enhance clinical variant interpretation in *KCNH2*-related long QT syndrome. Am. J. Hum. Genet.
16. Ficker, E., Dennis, A.T., Wang, L., and Brown, A.M. (2003). Role of the cytosolic chaperones Hsp70 and Hsp90 in maturation of the cardiac potassium channel HERG. Circ. Res. *92*, e87–e100. https://doi.org/10.1161/01.res.0000079028.31393.15.
17. Ioannidis, N.M., Rothstein, J.H., Pejaver, V., Middha, S., McDonnell, S.K., Baheti, S., Musolf, A., Li, Q., Holzinger, E., Karyadi, D., et al. (2016). REVEL: an Ensemble method for predicting the pathogenicity of rare missense variants. Am. J. Hum. Genet. *99*, 877–885. https://doi.org/10.1016/j.ajhg.2016.08.016.
18. Zhang, X., Walsh, R., Whiffin, N., Buchan, R., Midwinter, W., Wilk, A., Govind, R., Li, N., Ahmad, M., Mazzarotto, F., et al. (2021). Disease-specific variant pathogenicity prediction significantly improves variant interpretation in inherited cardiac conditions. Genet. Med. *23*, 69–79. https://doi.org/10.1038/s41436-020-00972-3.
19. Schlebach, J.P., and Sanders, C.R. (2015). The safety dance: biophysics of membrane protein folding and misfolding in a cellular context. Q. Rev. Biophys. *48*, 1–34. https://doi.org/10.1017/s0033583514000110.
20. Zhou, Y., and Bowie, J.U. (2000). Building a thermostable membrane protein. J. Biol. Chem. *275*, 6975–6979. https://doi.org/10.1074/jbc.275.10.6975.
21. Yue, P., Li, Z., and Moult, J. (2005). Loss of protein structure stability as a major causative factor in monogenic disease. J. Mol. Biol. *353*, 459–473. https://doi.org/10.1016/j.jmb.2005.08.020.
22. Wang, Z., and Moult, J. (2001). SNPs, protein structure, and disease. Hum. Mutat. *17*, 263–270. https://doi.org/10.1002/humu.22.
23. Anderson, C.L., Delisle, B.P., Anson, B.D., Kilby, J.A., Will, M.L., Tester, D.J., Gong, Q., Zhou, Z., Ackerman, M.J., and January, C.T. (2006). Most LQT2 mutations reduce Kv11.1 (hERG) current by a class 2 (trafficking-deficient) mechanism. Circulation *113*, 365–373. https://doi.org/10.1161/circulationaha.105.570200.
24. Brnich, S.E., Abou Tayoun, A.N., Couch, F.J., Cutting, G.R., Greenblatt, M.S., Heinen, C.D., Kanavy, D.M., Luo, X., McNulty, S.M., Starita, L.M., et al. (2020). Recommendations for application of the functional evidence PS3/BS3 criterion using the ACMG/AMP sequence variant interpretation framework. Genome Med. *12*, 3. https://doi.org/10.1186/s13073-019-0690-2.
25. Ng, C.A., Phan, K., Hill, A.P., Vandenberg, J.I., and Perry, M.D. (2014). Multiple interactions between cytoplasmic domains regulate slow deactivation of Kv11.1 channels. J. Biol. Chem. *289*, 25822–25832. https://doi.org/10.1074/jbc.m114.558379.
26. Perry, M.D., Ng, C.A., Phan, K., David, E., Steer, K., Hunter, M.J., Mann, S.A., Imtiaz, M., Hill, A.P., Ke, Y., and Vandenberg, J.I. (2016). Rescue of protein expression defects may not be enough to abolish the pro-arrhythmic phenotype of long QT type 2 mutations. J. Physiol. *594*, 4031–4049. https://doi.org/10.1113/jp271805.
27. Anderson, C.L., Routes, T.C., Eckhardt, L.L., Delisle, B.P., January, C.T., and Kamp, T.J. (2020). A rapid solubility assay of protein domain misfolding for pathogenicity assessment of rare DNA sequence variants. Genet. Med. *22*, 1642–1652. https://doi.org/10.1038/s41436-020-0842-1.
28. Morais Cabral, J.H., Lee, A., Cohen, S.L., Cohen, S., Chait, B.T., Chait, B., Li, M., and Mackinnon, R. (1998). Crystal structure and functional analysis of the HERG potassium channel N terminus. Cell *95*, 649–655. https://doi.org/10.1016/s0092-8674(00)81635-9.
29. Miosge, L.A., Field, M.A., Sontani, Y., Cho, V., Johnson, S., Palkova, A., Balakishnan, B., Liang, R., Zhang, Y., Lyon, S., et al. (2015). Comparison of predicted and actual consequences of missense mutations. Proc. Natl. Acad. Sci. U S A *112*, E5189–E5198. https://doi.org/10.1073/pnas.1511585112.
30. Wilcox, E.H., Sarmady, M., Wulf, B., Wright, M.W., Rehm, H.L., Biesecker, L.G., and Abou Tayoun, A.N. (2021). Evaluating the impact of in silico predictors on clinical variant classification. Genet. Med. *24*, 924–930. https://doi.org/10.1016/j.gim.2021.11.018.

31. Walsh, R., Lahrouchi, N., Tadros, R., Kyndt, F., Glinge, C., Postema, P.G., Amin, A.S., Nannenberg, E.A., Ware, J.S., Whiffin, N., et al. (2021). Enhancing rare variant interpretation in inherited arrhythmias through quantitative analysis of consortium disease cohorts and population controls. Genet. Med. *23*, 47–58. https://doi.org/10.1038/s41436-020-00946-5.

32. Feng, L., Zhang, J., Lee, C., Kim, G., Liu, F., Petersen, A.J., Lim, E., Anderson, C.L., Orland, K.M., Robertson, G.A., et al. (2021). Long QT syndrome *KCNH2* variant induces hERG1a/1b subunit imbalance in patient-specific induced pluripotent stem cell-derived cardiomyocytes. Circ. Arrhythmia Electrophysiol. *14*, e009343. https://doi.org/10.1161/circep.120.009343.